

## Analytical Chemistry

DNA Biomaterial Based Fiber Optic Sensor: Characterization and Application for Monitoring *in situ* Mercury PollutionNabarun Polley,<sup>[a]</sup> Probir Kumar Sarkar,<sup>[a]</sup> Subhananda Chakrabarti,<sup>[b]</sup> Peter Lemmens,<sup>[c]</sup> and Samir Kumar Pal<sup>\*[a]</sup>

In recent years considerable efforts have been devoted to utilize DNA based biomaterials for efficient sensor design. The polymeric molecule has high aqueous solubility, thus design of any water based sensor with DNA without rigorous chemical treatment (modification for covalent bonding) is challenging. In the present work we have developed a novel silver-nanoparticle (Ag-NPs) impregnated genomic DNA-lipid (CTAB) complex, which is completely insoluble in water and forms excellent thin film on optical fiber tips. The intact structural as well as functional integrity of the genomic DNA in the thin film

is found to be a key factor for its specific affinity to mercury ions in aqueous environments. We have demonstrated that a dip-coated optical fiber tip can work as a fluorescence sensor in addition to a surface plasmon resonance (SPR) type absorption sensor due to nano surface energy transfer (NSET) between the DNA minor-groove binding dye 4', 6-diamidino-2-phenylindole (DAPI) and Ag-NPs. Nanomolar, specific detection of mercury ions with few seconds reaction time is found in this versatile and economic way revealing clearly the advantageous aspects of our work.

## Introduction

DNA, 'the molecule of life' has been used extensively for the development of biomaterials in the last decade.<sup>[1]</sup> Applications of the biomaterial covers fully functional equivalents of the majority of electronic and photonics elements like light emitting diodes (LED), photovoltaic cells, transistors, memory chips, waveguides, laser, holographic gratings, elements of non-linear optics etc.<sup>[2]</sup> Among the different types of DNA based biomaterials the water insoluble DNA-lipid (surfactant) complex, produced upon reaction between DNA and a cationic surfactant<sup>[3]</sup> (such as, cetyltrimethyl ammonium chloride: CTMA or cetyltrimethyl ammonium bromide: CTAB) is most popular. The optical properties including high transmission (~100% at  $\lambda = 300\text{--}1600\text{ nm}$ ),<sup>[3]</sup> low optical loss (0.05 dB/cm at  $\lambda = 800\text{ nm}$ ) and favorable index of refraction (1.535 at  $\lambda = 350\text{ nm}$ )<sup>[4]</sup> of the thin film motivate many optoelectronic applications of this material.<sup>[4-5]</sup> In recent years considerable efforts have been devoted to utilize the materials as a sensor. Such as, dual detection of ultraviolet and visible light,<sup>[6]</sup> chemical sensing using

thin films as wave guides,<sup>[7]</sup> development of a metal-biopolymer-metal photodiode.<sup>[8]</sup> On the other hand, optical fiber sensors (OFS) are popular since 1987.<sup>[9]</sup> In a few recent reviews, the development of Fiber-Optic Chemical Sensors (FOCS) and Biosensors (FOBS) has been summarized.<sup>[10]</sup> Sensing by FOCS and FOBS includes temperature, humidity, different gases (oxygen, hydrogen, nitrogen, ammonia, carbon dioxide etc), glucose, salinity and others.<sup>[11]</sup> However, reports on elemental analysis like heavy metal ions dissolved in water is limited in the contemporary literature. There are few reports on potential FOS tools for the detection of mercury,<sup>[12]</sup> with limited portability, versatility and cost-effectiveness. Though there are several reports on the solution based efficient mercury sensors,<sup>[13]</sup> however, we have restricted our study in the development of *in situ* optical fiber based detection strategies. In the present work we have used a DNA based thin film on the tips of optical fibers for specific sensing of mercury ions ( $\text{Hg}^{2+}$ ) in dissolved water with 9 nM (~1.8 ppb) detection limit. The nano surface energy transfer (NSET) between 4', 6-diamidino-2-phenylindole (DAPI), an efficient DNA minor-groove binding luminescent dye and silver-nanoparticle (Ag-NPs) in the thin film plays the key role in the nanomolar specific detection of  $\text{Hg}^{2+}$  in aqueous environments. Since, no external processing (sample collection, preparation, handling and measurement) is required, FOS based mercury sensor is highly efficient for field measurements in natural waters in contrast to the kits based *ex situ* measurement with standard field portable equipment. Additionally, in the kits based system the presence of an expert is required due to its very precise sample preparation process (which is the main source of erroneous results). Whereas, FOS based system can be handled by any non expert with little or no knowledge of instrument handling.

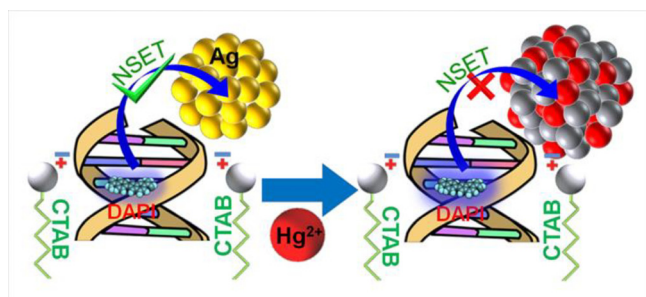
[a] N. Polley, P. K. Sarkar, Prof. S. K. Pal  
Department of Chemical, Biological and Macromolecular Sciences  
S. N. Bose National Centre for Basic Sciences  
Block JD, Sector III, Salt Lake, Kolkata 700 106 (India)  
E-mail: skpal@bose.res.in

[b] Prof. S. Chakrabarti  
Dept. of Electrical Engineering  
Indian Institute of Technology Bombay  
Powai, Mumbai 400 076, Maharashtra, India

[c] Prof. P. Lemmens  
Institute for Condensed Matter Physics  
TU Braunschweig, Mendelssohnstr 3, 38106 Braunschweig, Germany

Supporting information for this article is available on the WWW under <http://dx.doi.org/10.1002/slct.201600391>

DNA, the polymeric molecule with two intertwined spirals of sugar and phosphate molecules linked by hydrogen-bonded base pairs is shown to be useful in developing novel nanostructured materials.<sup>[14]</sup> Structural properties of biopolymers including DNA often have unusual properties that are not easily replicated using conventional organic or inorganic materials.<sup>[1–2]</sup> Moreover, they are abundant in nature and can easily be degraded without causing any harm to the environment. In our study, we have used the salmon sperm DNA which is a waste product of fish-processing industry. The DNA is highly soluble in water but forms complex polymers upon interaction with cationic surfactants. The complex is insoluble in water but soluble in alcohol,<sup>[15]</sup> which is advantageous not only in terms of casting DNA thin-films over any surface but also ideal for sensing analytes in water. We have utilized the exceptional affinity of DNA towards different dyes to insert DAPI<sup>[16]</sup> into the DNA (DNA-DAPI). Furthermore using DNA for templating inorganic nanostructures has been frequently reported in recent years.<sup>[17]</sup> We have used DNA to impregnate silver nanoparticles (Ag-NPs) during the complexation reaction with surfactant CTAB. The lyophilized powder of DNA-DAPI-CTAB-Ag-NPs complex is dissolved in ethanol. Upon characterization of the thin film by optical spectroscopy and imaging, we have dip-coated a chemically etched fiber tip for sensing mercury ( $\text{Hg}^{2+}$ ) in water. The regenerative use of the fiber tip can be achieved by removing the coating using ethanol followed by further dip-coating of the tip. The phenomenon of nano surface energy transfer (NSET) in the bio-material of DNA-DAPI with Ag-NPs reduces the emission of DAPI significantly (Scheme 1). Upon interaction



**Scheme 1.** Schematic representation of the nano surface energy transfer (NSET) between DNA-DAPI and silver nanoparticles (Ag-NPs) and De-NSET upon interaction with mercury ( $\text{Hg}^{2+}$ ) due to amalgamation of Ag-NPs with  $\text{Hg}^{2+}$ .

of Ag-NPs in the fiber tip with the  $\text{Hg}^{2+}$  the Ag-NPs in the film undergoes an amalgamation reaction with  $\text{Hg}^{2+}$  and eventually lose the surface plasmon resonance (SPR) (Scheme 1). We have shown that the decrease in SPR, at the fiber tip has strong dependency on the  $\text{Hg}^{2+}$  concentration in the test water. On the other hand, due to the absence of the acceptor, SPR of the Ag-NPs, the emission of DAPI in the film is restored.

## Results and Discussion

**Characterizing the Bio-film material by HRTEM and SEM:** Figure 1(a) presents a TEM image of Ag-NPs impregnated bio-

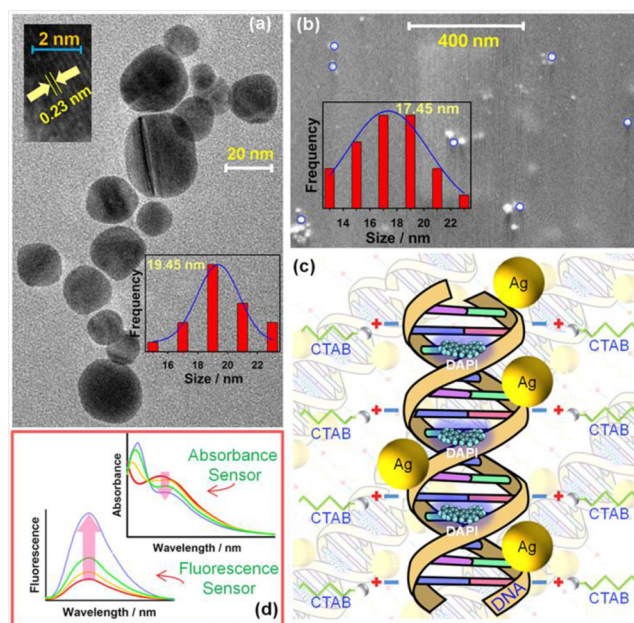


**Figure 1.** (a) TEM image of Ag-NPs impregnated DNA-DAPI bio-film. (a-Upper inset) Lattice fringes in the corresponding HRTEM image indicating high crystalline nature of the Ag-NPs. (a-Lower inset) Size distribution of Ag-NPs in the bio-film. (b) SEM image of Ag-NPs impregnated DNA-DAPI bio-film. (b-inset) Size distribution of Ag-NPs in the bio-film. (c) Schematic representation of the bio-film based on spectroscopic and imaging studies. (d) Potential application of the bio-film has been schematically represented.

films. It is found that Ag-NPs are spherical in shape with an average diameter of 19.45 nm, which is slightly large compare to earlier results of the followed synthesis procedure.<sup>[18]</sup> A reason for that could be an interaction of the citrate capped Ag-NPs with CTAB during the preparation of the bio-films.<sup>[19]</sup> However, no change in the particle size distribution (lower inset of the Figure 1(a)) is observed even after few months from the synthesis of the bio-film material. The HRTEM image (Upper inset Figure 1(a)) has provided us further insight into the microstructure and crystallinity of the Ag-NPs in the bio-films. The high crystalline nature of the Ag-NPs with lattice spacing of 0.23 nm corresponds to (111) planes of silver, which further corroborates the (111) planes as dominant faces of the silver spheres. The SEM image of the bio-film upon casting on a silicon wafer is shown in Figure 1(b). The spherical Ag-NPs with an average diameter of 17.45 nm are observed on the surface of the film. The particle size distribution is represented in the inset of Figure 1(b). The apparent decrease in diameter of Ag-NPs compare to the TEM measurement is observed due to the fact that all the particles are submerged in the film and we are able to see only the rise part of the Ag-NPs. From both observations, in Figure 1(a) and 1(b), the structure of the bio-films is represented schematically in Figure 1(c). The water insoluble

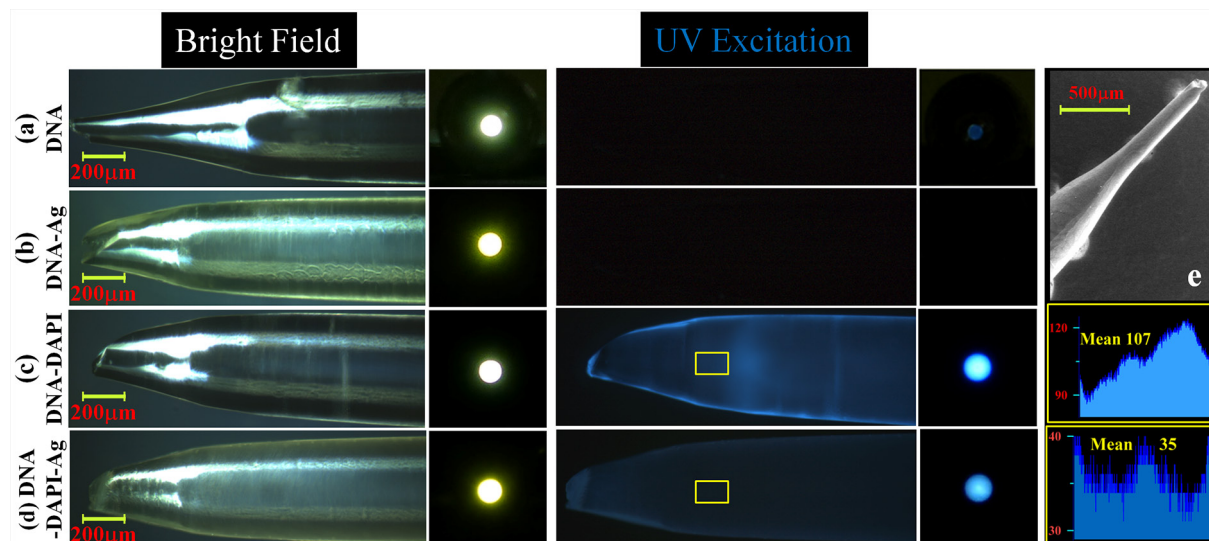


**Figure 2.** The comparative study of different bio-film coated fiber tips under bright field (Integration time ( $t$ ) = 20 ms) and UV excitation ( $t$  = 100 ms) (a) DNA, (b) DNA–Ag-NPs, (c) DNA-DAPI, (d) DNA-DAPI–Ag-NPs. The adjacent images represent the image of the other fiber end (Bright field  $t$  = 10 ms, UV excitation  $t$  = 40 ms). The rectangles on the right represent the blue channel area histogram data corresponding to the RGB analysis of the highlighted portions of (c) and (d). (e) SEM image of bio-film coated fiber optic sensor tip.

DNA-CTAB complex is formed due to the binding of CTAB cationic polar head to the negative phosphate sugar chain of the DNA strands. During the binding process of DNA with CTAB it impregnates Ag-NPs in the solution and precipitates. So the overall view of the bio-material should be Ag-NPs are embedded in the water insoluble DNA-CTAB complex. We have highlighted only a section of the matrix in Figure 1(c) for clarity. Since the DNA is tagged with DAPI, the biomaterial fluoresce around 440 nm<sup>[16]</sup> under UV excitation. On the other hand the Ag-NPs have a SPR band around 400 nm.<sup>[18]</sup> Thus a strong overlap between the emission spectra of DNA-DAPI and SPR of Ag-NPs suggests the possibility of energy transfer (ET) upon close proximity, which could be utilized for sensing. Possible applications of the bio-films have been summarized pictorially in Figure 1(d). Upon perturbation of the SPR band of Ag-NPs leads to change in color of the bio-films (absorbance) as well as fluorescence of the material, both can be utilized in sensing applications.

**Microscopic Characterization of the bio-film coated fiber tips:** The comparative study of different bio-film coated fiber tips under bright field and UV excitation is represented in Figure 2 (Integration time (IT) for photographic image; Bright field = 20 ms, UV Excitation = 100 ms). In this study the fiber tips were first dip-coated with the desired bio-film and placed under microscope. During imaging the light coupled into the fiber through the tip and transmitted all the way to the other end of the fiber, image of this end (Bright field IT = 10 ms, UV excitation IT = 40 ms) of the fiber is represented in adjacent to each fiber tip images. We have considered four variants of bio-film DNA (a), DNA–Ag-NPs (b), DNA-DAPI (c), DNA-DAPI–Ag-NPs (d) (CTAB is common for all). (a) and (b) both are invisible under UV excitation since there is no fluorescence but under bright field (b) is yellowish compare to (a) due to the presence

of Ag-NPs in the tip. Since the Ag-NPs in the tip acts as a filter, for (b) the other end of the fiber is observed as bright yellow. In case of (c) and (d) the observation under bright field is the same as (a) and (b) respectively due to the same reason (presence of Ag-NPs in (d)) but they are both visible under UV excitation because of the DNA intercalating dye DAPI. Though the concentration of DAPI present in both the films are same but (d) fluoresce less due to the presence of Ag-NPs in the film, which indicates the possibility of energy transfer between the DAPI and Ag-NPs in the film. The corresponding image of the fiber ends shows that the intensity of (d) is much less compare to (c). This is also reflected in the RGB (red-green-blue) analysis of the selected area ((c) and (d) Yellow rectangle) of the fiber tip images under UV excitation. The blue channel data corresponding to the area histogram of the selected portions, represented in the Figure 2 (Left, yellow rectangle) reveals that the average blue channel intensity for (c) is 107 whereas for (d) it is 35 only. The SEM image of the bio-film coated fiber tip is represented in Figure 2(e).

**Spectroscopic Characterization of the bio-film coated fiber:** The experimental set up (Figure 3) was used for the testing upon dip coating the optical fibers with the bio-material (details in the experimental section). The absorbance spectra of the DNA-DAPI-CTAB–Ag-NPs (DNA–D–Ag, Figure 4) film obtained in the experimental setup is represented in Figure 4 (a). The SPR of the Ag-NPs is clearly observed, peaking at a wavelength of 400 nm. The spectra of the bio-film material (in ethanol) recorded in spectrophotometer is also provided in the inset of the Figure 4(a). Along with the SPR of Ag-NPs, the huge absorbance peak of the DNA at 260 nm is evident. The emission and excitation spectra of the bio-film recorded under the experimental setup (described in experimental section) are represented in the Figure 4(b). A strong blue (440 nm) emission is

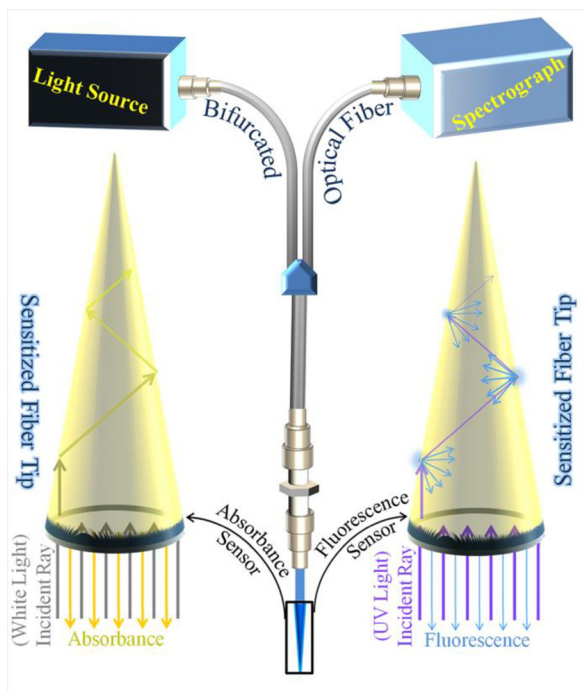


Figure 3. Schematic representation of the experimental setup.

observed with the excitation of 350 nm ( $\lambda_{\text{ex}} = 350$  nm). The excitation spectra corresponding to 440 nm ( $\lambda_{\text{em}} = 440$  nm) reveals the excitation wavelength at around 340 nm. The decrease in emission intensity with the presence of Ag-NPs (DNA–D–Ag) in the DNA–DAPI (DNA–D) bio-film is represented in the inset of Figure 1(b). Initially, time resolved Förster resonance energy transfer (FRET) technique was employed to detect and study the interaction of DNA–DAPI (DNA–D) with the Ag-NPs. Inset of Figure 4(c) shows the strong spectral overlap between the emission spectrum of DNA–DAPI (donor) and the SPR band of Ag-NPs (acceptor). Picosecond resolved photo luminescent transients (Figure 4c) of both donor and donor–acceptor systems, monitored at 440 nm, shows significant shortening in the DNA–DAPI fluorescence lifetime upon introduction of Ag-NPs in the system. The picosecond resolved fluorescence decay of DNA–DAPI in revealed multi-exponential time constants of 0.06 ns (29%), 0.742 ns (14%) and 2.61 ns (57%) giving an average time constant ( $\tau_{\text{avg}}$ ) of 1.61 ns. For the donor–acceptor system time constants are obtained as 0.03 ns (56%), 0.7 ns (11%) and 2.58 ns (33%) giving an average time constant ( $\tau_{\text{avg}}$ ) of 0.95 ns (Table 1). The substantial shortening in the excited state lifetime of DNA–DAPI upon conjugate formation indicates conclusively that efficient FRET could occur from the DNA–DAPI donor to the Ag-NPs acceptor. Considering the quantum yield of DNA–DAPI in absence of acceptor as 0.92<sup>[20]</sup> and based on the spectral overlap, we have estimated a FRET efficiency of 41% using Eq. (4). The measured donor–acceptor distance (R) calculated using Eq. (3) is 21 nm, which is greater than 100 Å. The phenomenon of Ag-NPs based surface energy transfer (SET) process serves as a ruler to unravel the distance range well beyond 10 nm, which follows  $1/d^4$  distance

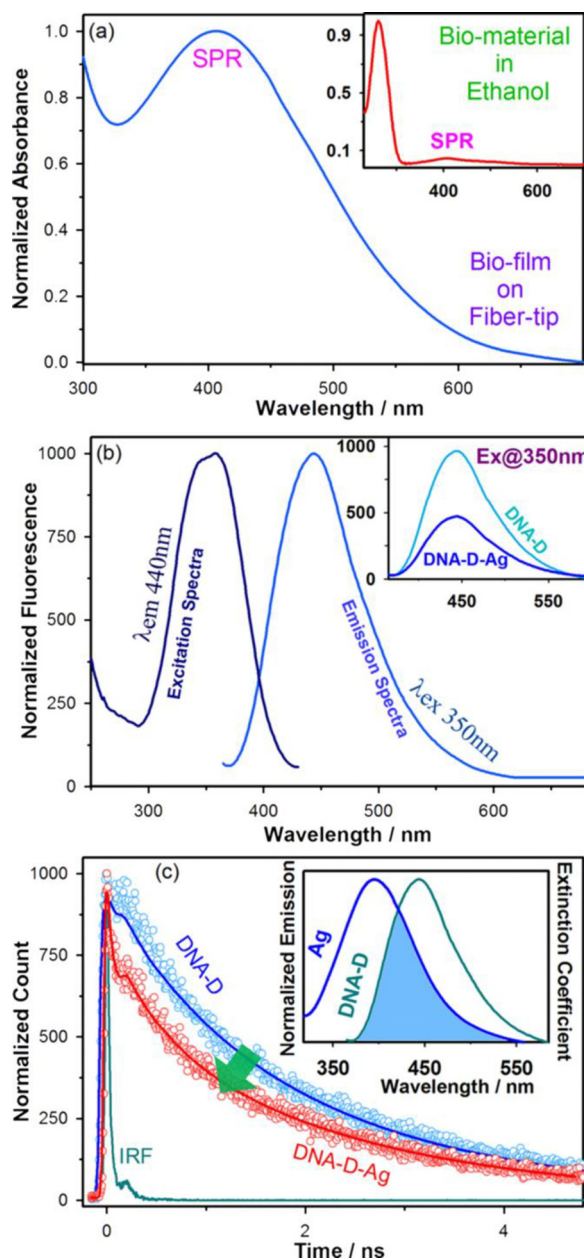


Figure 4. (a) The absorbance spectra of the bio-film obtained from the proposed experimental setup. (inset) The absorbance spectra of the bio-material in ethanol with the DNA peak at 260 nm. (b) The emission upon excitation at 350 nm ( $\lambda_{\text{ex}} = 350$  nm) and excitation spectra corresponding to 440 nm ( $\lambda_{\text{em}} = 440$  nm) of the bio-film obtained from the proposed experimental setup. (inset) The emission quenches due to presence of Ag-NPs in the DNA–DAPI bio-film. (c) Picosecond-resolved PL transients of DNA–DAPI (Blue), DNA–DAPI–Ag-NPs (Red) bio-material coated fiber tips and monitored at  $\lambda_{\text{em}} = 440$  nm. (inset) Spectral overlap between emission spectrum of DNA–DAPI and the surface plasmon resonance (SPR) band of Ag-NPs.

dependence.<sup>[21]</sup> In order to favor the NSET formulism, the distance between donor DAPI and acceptor Ag-NPs is calculated to be 8.05 nm ( $d_0 = 7.40$  nm) from equations (5) and (6), respectively. As the calculated donor–acceptor distance is in consonance with the size of the Ag-NPs (radius 10 nm), hence, it is worth emphasizing that the energy transfer from DAPI to Ag-

Figures	Description	$\tau_1$ [a]	$\tau_2$ [a]	$\tau_3$ [a]	$\tau_{avg}$ [a]
Figure 4c)	DNA-DAPI	0.06 (29%)	0.74 (14%)	2.61 (57%)	1.61
	DNA-DAPI–Ag-NPs	0.03 (56%)	0.70 (11%)	2.58 (23%)	0.95
Figure 5c)	DNA-DAPI–Ag-NPs	0.03 (56%)	0.70 (11%)	2.58 (23%)	0.95
	DNA-DAPI–Ag-NPs-Hg	0.1 (29%)	0.71 (18%)	2.25 (53%)	1.32

[a] Units in ns

NP results in the reduced DAPI emission as observed in the figures Figure 2 (variant d) and inset of Figure 4(b).

**Sensing application of the Bio-film coated fiber:** Sensitivity of the fiber sensor towards  $Hg^{2+}$  in water was first assessed through the absorbance pathway. The comparative kinetics (at 400 nm) of the SPR band with different concentration (9 nM, 90 nM, 500 nM, 900 nM, 1.4  $\mu$ M, 9  $\mu$ M, 25  $\mu$ M and 50  $\mu$ M) of mercury in water is represented in Figure 5(a). The reduction in the amplitude of SPR band with time upon interaction of the bio-film coated optical fiber sensor with  $Hg^{2+}$  with time is observed (Figure 5 (a) inset I). It has been also found that the change in absorbance is linearly proportional with the concentration of the mercury in the range of 0 to 1500 nM ((Figure 5(a) inset II,  $r=0.96$ , slope  $9.06 \times 10^{-5}$  and Y intercept 0.05). The Sensing ability of the bio-film coated tip sensor toward  $Hg^{2+}$  in water was also assessed through the fluorescence pathway. The emission kinetics (at 440 nm) of sensor with different concentration of mercury in the range mentioned above is represented in Figure 5(b). The increment in the intensity is clearly evident from the emission spectra obtained from the sensor (Figure 5(b) inset I). The linear dependency between the concentration of the mercury and intensity change establishes the potential of this detection mechanism ((Figure 5(b) inset II,  $r=0.99$ , slope 4.97 and y intercept 4345.62). In order to investigate the probable reaction pathway the decay transient of sensors after interaction with  $Hg^{2+}$  were recorded. The average excited state lifetime (Table 1) of the sensor recovered subsequently from 0.95 ns to 1.32 ns, (tending toward DNA-DAPI value of 1.61 ns without Ag-NPs) revealing the possibility of de-NSET mechanism in the fiber tip sensor (Figure 5(c)). Or in other words the state of the acceptor (Ag-NPs) is perturbed. The possible reasons could be that the Ag-NPs leave the film or it is present in the film but due to interaction with the  $Hg^{2+}$  it loses the SPR, the observed results are justified in both the cases. To have a better insight into the reaction mechanism following electron microscopic studies has been performed.

**The mechanism of action:** In order to investigate the mechanism of action we have performed the TEM, SEM as well as EDX study of the bio-film material before and after interaction with mercury ( $Hg^{2+}$ ). The TEM image (Figure 6(a) before

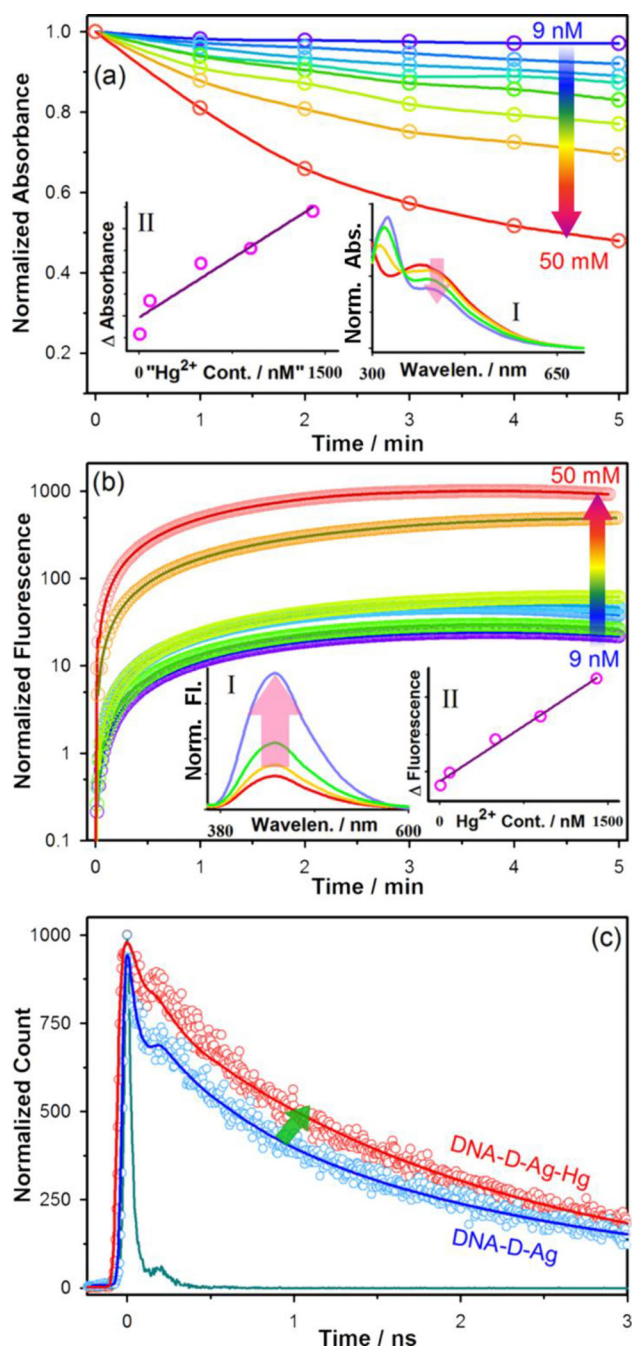


**Figure 5.** (a) & (b) Absorbance and fluorescence kinetics of the bio-film coated fiber tip with different concentration of mercury from 9 nM to 50  $\mu$ M respectively. (Inset a) & (Inset b) Reduction in amplitude of SPR band (absorbance) and increment in the emission of DAPI with time upon interaction of the sensor with mercury ( $Hg^{2+}$ ) respectively. (Inset aII) & (Inset bII) Change in absorbance and fluorescence is linearly proportional with the  $Hg^{2+}$  concentration in the range 0–1600 nM. (c) The De-NSET of the DNA-DAPI and Ag-NPs due the amalgamation of Ag-NPs with  $Hg^{2+}$ .

and 6(b) after) suggests that upon interaction with the  $Hg^{2+}$  the average particle size of Ag-NPs has drastically increased from 20 nm to more than 200 nm. Same characteristic change of Ag-NPs has been reflected from the SEM study of the bio-film material (Figure 6(c) before and 6(d) after). The EDX study

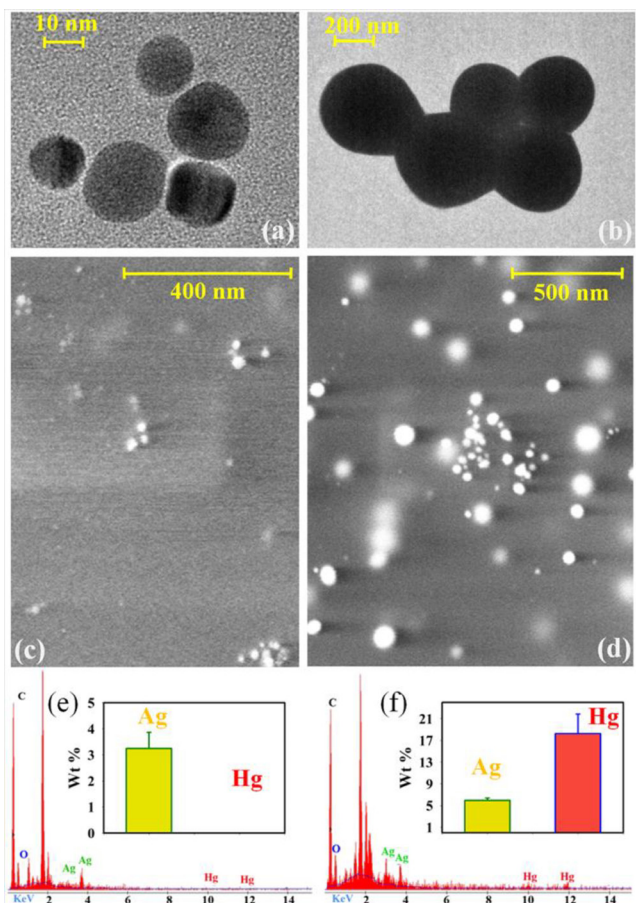


**Figure 6.** The TEM image of the Ag-NPs impregnated bio-film before and after interaction with  $\text{Hg}^{2+}$  (a) and (b) respectively. The SEM image of the Ag-NPs impregnated bio-film before and after interaction with mercury ions ( $\text{Hg}^{2+}$ ) (c) and (d) respectively. The EDX curve corresponding to the bio-films before and after interaction with  $\text{Hg}^{2+}$  with (inset) comparative presence (wt%) of silver (Ag) and mercury (Hg) in the bio-film.

of the bio-film (Figure 6(e) before and 6(f) after) reveals that though the amount of silver present in the film before and after the interaction remains almost same (4 wt%, Figure 6(e) and 6(f) inset) but the presence of  $\text{Hg}^{2+}$  increased from 0 wt% to 20 wt% (Figure 6(f) inset). The results clearly suggests that the Ag-NPs does not leave the film rather due to highly reactive nature of the  $\text{Hg}^{2+}$  it could be possible that they are undergoing for the amalgam formation. In earlier reports on silver nanoparticle based  $\text{Hg}^{2+}$  sensing, it has been concluded to form Ag–Hg amalgam<sup>[22]</sup>. The statement is also supported by the observation (Figure 5 (a) inset I) of simultaneous decrease in SPR peak due to larger NPs (~400 nm) followed by blue shift in the spectra due to the reduction of effective size of the NPs and formation bimetallic NPs<sup>[22]</sup>.

**The selectivity test:** The optical responses of the biosensor towards metal ions such as Ag (II), Ca(II), Cd(II), Co(II), Cu(II), Fe (II), K(I), Mg(II), Na(I), Ni(II), Pb(II), Zn(II), Hg(II), have been investigated. Among these ions, only Hg(II)/ $\text{Hg}^{2+}$  has a significant effect on the absorbance (Figure 7(a)) as well as in emission (Figure 7(b)) spectra of the bio-material. The changes of

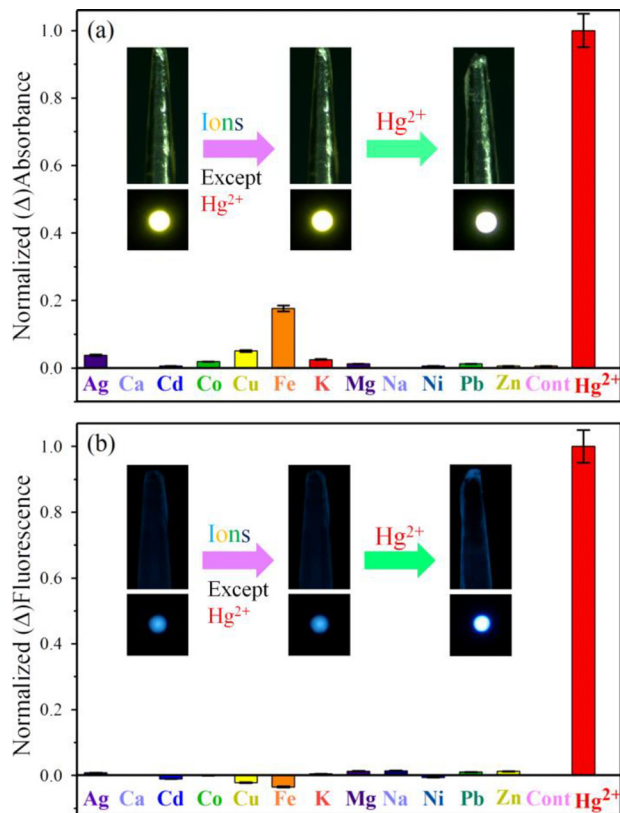


**Figure 7.** Specificity test of the bio-film coated fiber sensor towards  $\text{Hg}^{2+}$  in contrast to the other metal ions in both the absorbance and the fluorescence way is represented in (a) and (b) respectively. (a- inset) The disappearance (reduction) of SPR band of Ag-NPs in the bio-film upon interaction with mercury ions ( $\text{Hg}^{2+}$ ), (b-inset) the consequent increase in intensity of the bio-film is represented.

absorbance and fluorescence after the interaction (5 min) with different ions have been represented in Figure 7 with a 5% error bar. The high selectivity of the biosensor towards  $\text{Hg}^{2+}$  over other biologically relevant metal ions can be seen with the naked eye also (Figure 7, insets). The disappearance (or reduction) of SPR band of Ag-NPs in the bio-film upon interaction with  $\text{Hg}^{2+}$  (Figure 7(a) inset) and consequent increase in intensity (Figure 7(b) inset) is evident from the images obtained from microscopic studies.

## Conclusions

In summary, we have developed a DNA-based optical fiber sensor for the in situ measurement of mercury pollution with nM detection efficiency. Impregnated citrate capped silver nanoparticles (Ag-NPs ~20 nm) in a water insoluble DNA-lipid complex at the tip of a multimodal optical fiber is shown to play crucial role in the ultra-sensitive sensing mechanism. While, loss of SPR of the Ag-NPs in the proximity of mercury ions due to amalgamation and size enhancement is shown to be a key factor for the absorption based-sensing. Simultaneous de-NSET from a minor groove binding dye (DAPI) to the impregnated Ag-NPs (due to amalgamation) revealing restoration of DAPI

fluorescence in presence of  $\text{Hg}^{2+}$  ions is an important mechanism for fluorescence based sensing. Our study clearly shows that the sensor is extremely selective to mercury ions, even in presence of other interfering cations generally present in water of natural sources. We have also developed a prototype of the system for potential field trials.

## Supporting information

General experimental details including the synthesis procedures of optical fibers, experimental setup, mathematical tools for calculating the donor-acceptor distance can be found in Supporting Information.

## Acknowledgements

N.P thanks DST, India for Inspire Research Fellowship and P.K.S thanks UGC, India for providing fellowship under the UGC-RGNF scheme. We thank DST, India for financial grants (DST/TM/SERI/2k11/103, SB/S1/PC-011/2013), NTH-School "Contacts in Nanosystems: Interactions, Control and Quantum Dynamics", the Braunschweig International Graduate School of Metrology (IGSM), and DFG-RTG 1952/1, Metrology for Complex Nanosystems.

**Keywords:** DNA based Nanomaterials · Nano-sensor · Fiber optic sensor · SPR-sensor · NSET-sensor

- [1] A. J. Steckl, *Nat Photon* **2007**, *1*, 3–5.
- [2] J. Nizioł, M. Śniechowski, in *Transparent Optical Networks (ICTON), 2014 16th International Conference on*, IEEE, **2014**, pp. 1–4.
- [3] K. Tanaka, Y. Okahata, *J. Am. Chem. Soc.* **1996**, *118*, 10679–10683.
- [4] J. A. Hagen, University of Cincinnati **2006**.
- [5] J. Shinar, V. Savvateev, in *Organic Light-Emitting Devices* (Ed.: J. Shinar), Springer New York, **2004**, pp. 1–41.
- [6] M. S. P. Reddy, B.-J. Kim, J.-S. Jang, *Opt. Express* **2014**, *22*, 908–915.
- [7] P. P. Yaney, E. M. Heckman, D. E. Diggs, F. K. Hopkins, J. G. Grote, in *Proc. SPIE-Int. Soc. Opt. Eng.*, Vol. 5724, **2005**, pp. 224–233.
- [8] B. Zhou, S. J. Kim, C. M. Bartsch, E. M. Heckman, F. Ouchen, A. N. Cartwright, Vol. 8103, **2011**, pp. 810308–810308-810312.
- [9] C. A. Villarruel, D. D. Dominguez, A. Dandridge, Vol. 0798, **1987**, pp. 225–229.
- [10] a) O. S. Wolfbeis, *Anal. Chem.* **2008**, *80*, 4269–4283; b) X.-D. Wang, O. S. Wolfbeis, *Anal. Chem.* **2013**, *85*, 487–508; c) M. Pospíšilová, G. Kuncová, J. Trögl, *Sensors* **2015**, *15*, 25208–25259; d) X.-d. Wang, O. S. Wolfbeis, *Anal. Chem.* **2016**, *88*, 203–227.
- [11] a) R. Verma, B. D. Gupta, *Analyst* **2013**, *138*, 7254–7263; b) I. Sergachev, A. Rusanov, E. Trushkin, D. Sakharov, U. Marx, A. Tonevitsky, *Analyst* **2013**, *138*, 4066–4069.
- [12] a) X.-B. Zhang, C.-C. Guo, Z.-Z. Li, G.-L. Shen, R.-Q. Yu, *Anal. Chem.* **2002**, *74*, 821–825; b) M. Yin, B. Gu, J. Qian, A. P. Zhang, Q. An, S. He, *Anal. Methods* **2012**, *4*, 1292–1297; c) J. S. Crosby, D. Lucas, C. P. Koshland, *Sensor. Actuat. B-Chem.* **2013**, *181*, 938–942; d) K. Bhavsar, R. Prabhu, P. Pollard, *P. J. Phys.: Conf. Ser.* **2013**, *450*, 012011; e) F. Long, C. Gao, H. C. Shi, M. He, A. N. Zhu, A. M. Klibanov, A. Z. Gu, *Biosens. Bioelectron.* **2011**, *26*, 4018–4023.
- [13] a) A. Ono, H. Togashi, *Angew. Chem. Int. Ed.* **2004**, *43*, 4300–4302; b) C.-C. Huang, Z. Yang, K.-H. Lee, H.-T. Chang, *Angew. Chem.* **2007**, *119*, 6948–6952; c) H. Dai, F. Liu, Q. Gao, T. Fu, X. Kou, *Luminescence* **2011**, *26*, 523–530; d) N. Goswami, A. Giri, S. Kar, M. S. Bootharaju, R. John, P. L. Xavier, T. Pradeep, S. K. Pal, *Small* **2012**, *8*, 3175–3184.
- [14] N. C. Seeman, *Nature* **2003**, *421*, 427–431.
- [15] V. G. Sergeev, S. V. Mikhailenko, O. A. Pyshkina, I. V. Yaminsky, K. Yoshikawa, *J. Am. Chem. Soc.* **1999**, *121*, 1780–1785.
- [16] D. Banerjee, S. K. Pal, *J. Phys. Chem. B* **2008**, *112*, 1016–1021.
- [17] a) S. M. D. Watson, A. R. Pike, J. Pate, A. Houlton, B. R. Horrocks, *Nanoscale* **2014**, *6*, 4027–4037; b) S. M. D. Watson, H. D. A. Mohamed, B. R. Horrocks, A. Houlton, *Nanoscale* **2013**, *5*, 5349–5359; c) G. Shemer, O. Krichevski, G. Markovich, T. Molotsky, I. Lubitz, A. B. Kotlyar, *J. Am. Chem. Soc.* **2006**, *128*, 11006–11007.
- [18] C. Y. Flores, C. Diaz, A. Rubert, G. A. Benítez, M. S. Moreno, M. A. Fernández Lorenzo de Mele, R. C. Salvarezza, P. L. Schilardi, C. Vericat, *J. Colloid Interface Sci.* **2010**, *350*, 402–408.
- [19] Z. M. Sui, X. Chen, L. Y. Wang, L. M. Xu, W. C. Zhuang, Y. C. Chai, C. J. Yang, *Phys. E* **2006**, *33*, 308–314.
- [20] a) J. Kapuscinski, *Biotech. Histochem.* **1995**, *70*, 220–233; b) N. Polley, S. Singh, A. Giri, P. K. Mondal, P. Lemmens, S. K. Pal, *Sensor. Actuat. B-Chem.* **2015**, *210*, 381–388.
- [21] a) M. A. H. Muhammed, A. K. Shaw, S. K. Pal, T. Pradeep, *J. Phys. Chem. C* **2008**, *112*, 14324–14330; b) P. K. Sarkar, N. Polley, S. Chakrabarti, P. Lemmens, S. K. Pal, *ACS Sens.* **2016**, *1*, 789–797; c) S. Chaudhuri, S. Sardar, D. Bagchi, S. S. Singha, P. Lemmens, S. K. Pal, *J. Phys. Chem. A* **2015**, *119*, 4162–4169.
- [22] a) L. Deng, X. Ouyang, J. Jin, C. Ma, Y. Jiang, J. Zheng, J. Li, Y. Li, W. Tan, R. Yang, *Anal. Chem.* **2013**, *85*, 8594–8600; b) G. V. Ramesh, T. P. Radhakrishnan, *ACS Appl. Mater. Interfaces* **2011**, *3*, 988–994; c) G. Chen, Z. Guo, G. Zeng, L. Tang, *Analyst* **2015**, *140*, 5400–5443.

Submitted: April 14, 2016

Accepted: July 1, 2016